Tetrabenzo[*ab*,*f*,*jk*,*o*][18]annulene: synthesis, crystal structure analysis, *ab initio* quantum-chemical studies of intermolecular interactions in the gas phase and in crystalline states, photodimerization and photopolymerization

Richeng Yu,[a] Alexander Yakimansky,†[a] Ingrid G. Voigt-Martin,*[a] Michael Fetten,[b] C. Schnorpfeil,[b] Dieter Schollmeyer[b] and Herbert Meier[b]

[a] *Johannes-Gutenberg-Universität, Institut für Physikalische Chemie, Welder Weg 11, D-55099 Mainz, Germany*
[b] *Johannes-Gutenberg-Universität, Institut für Organische Chemie, Duesbergweg 10-14, D-55099 Mainz, Germany*

Received (in Cambridge, UK) 2nd March 1999, Accepted 25th June 1999

The synthesized title compound **8** crystallizes in three different modifications, which were investigated by electron crystallography, high resolution electron microscopy and X-ray structural analysis. The formation of molecular pairs was studied by an *ab initio* quantum-chemical approach. The calculated "dimers" were compared to the mutual orientations of nearest neighboring molecules in the crystal structures and to covalently bonded dimers obtained by a topochemical photodimerization.

1. Introduction

Areno-condensed annulenes represent a class of compounds with interesting photophysical and photochemical properties.[1–5] Due to their high thermal and chemical stability these compounds can be applied in materials science, particularly in the field of liquid crystals and photoconductivity.

Because of the dependence of the physical and chemical behavior on the molecular and supramolecular structure we synthesized and investigated tetrabenzo[*ab*,*f*,*jk*,*o*]cyclooctadecene (**8**) as a model compound. It is a formal [18]annulene, which is condensed with four benzene rings—two are linked in *ortho* and two in *meta* positions. Thus it is closely related to the naphtho-, phenanthro- and chryseno-condensed [18]annulenes described earlier.[1–5]

In order to understand the aggregation tendency[2] and the photochemistry, the crystal structures of **8** were investigated using electron crystallography, high resolution electron microscopy and X-ray analysis. The possibility of dimerization of these molecules in the gas-phase or in solution was studied by an *ab initio* quantum-chemical approach. The calculated geometries of the most stable gas-phase dimers were compared with the mutual orientations of the nearest neighboring molecules in the crystal structures and related to the observed photodimers which are covalently bonded.

2. Methods

2.1 Preparation and characterization of tetrabenzo[*ab*,*f*,*jk*,*o*]-[18]annulene by ^{1}H NMR spectroscopy

3-Bromobenzaldehyde (**1**) was protected as acetal **2** and then transformed by a Bouveault reaction in high yield to the aldehyde **3**. The (*E*)-configured stilbene **6** was formed by a Wittig–Horner reaction of **3** and the phosphonic ester **5** which could be obtained from 1-chloromethyl-2-methylbenzene (**4**) and triethyl phosphite. The reaction of **6** with aniline led in quantitative yield to the *N*-phenylimine **7** which showed in a strongly alkaline medium a cyclocondensation reaction to the title compound **8** (Scheme 1). Linear condensation products, that still contain polar imino groups, could be easily separated due to their better solubility in polar solvents. The generation of the two olefinic double bonds in the final step is highly stereoselective; no trace of a (*Z*)-configured isomer could be detected in the ^{1}H NMR spectrum.

Compound **8**, a formal derivative of [18]annulene, has to be considered—like related areno-condensed annulenes[1–5]—as a system of aromatic ring islands combined by olefinic bridges. A macrocyclic aromaticity can be excluded.[3] The NOE measurements permit the exact correlation of the ^{1}H NMR signals to certain protons and thus reveal that the inner protons 5-H ($\delta = 7.83$) and 23-H ($\delta = 8.29$) generate signals at somewhat lower field than the outer protons 4-H ($\delta = 7.08$); a macrocyclic aromaticity can be excluded. The fixing of the olefinic double bonds is also documented by the vicinal coupling constant ^3J (4-H, 5-H) of 16.1 Hz which is characteristic of the *trans* configuration.

2.2 Electron diffraction

For electron diffraction extremely small crystals are required. These were grown by dissolving **8** in toluene at 80 °C, crystallizing for 1 hour and subsequently quenching. The crystal modification gained by this procedure is called **A**.

The samples were investigated in a Philips EM-300 electron microscope with a eucentric goniometer stage. The individual crystals can be rotated and tilted up to ±60°. Details of the experimental and theoretical procedures have been published in several papers.[6–12] A short resume is given below.

(1) The basic zone is established by tilting about significant axes and determining the positions corresponding to the largest *d*-spacing. (2) An axis with strong reflections is established and chosen as the tilt axis. Upon tilting, the diffraction pattern first disappears and then reappears when a new zonal projection appears, the angle is noted and the process is repeated. The tilting is always performed both to the right and to the left direction. (3) A second axis is chosen as the tilt axis and the procedure repeated.

† Permanent address: Institute of Macromolecular Compounds of Russian Academy of Sciences, Bolshoi pr. 31, 199004 St. Petersburg, Russia.

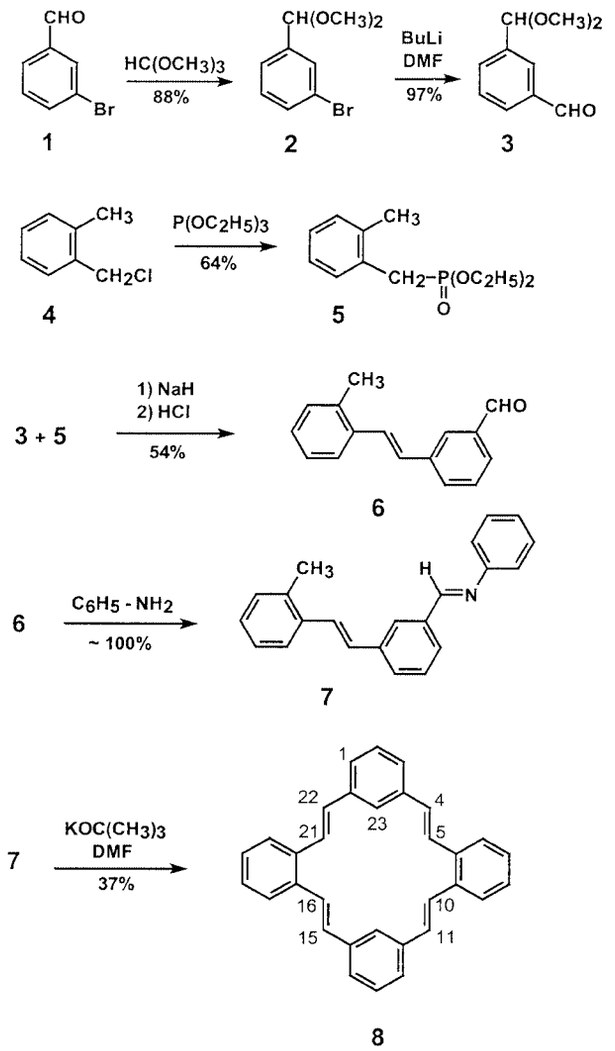

Scheme 1

The diffraction patterns are scanned into a PC where they are evaluated using the program ELD.[6–12]

From the diffraction patterns the unit cell dimensions can be determined. On the basis of extinctions observed in different projections, it is generally possible to reduce the number of possible space groups to two or three. By subsequent molecular modeling, the possible number of space groups can normally be further reduced.

The recent successful structure determinations using direct methods,[13] maximum entropy statistics and/or simulations[6–12] based on electron diffraction data demonstrate that the methods all work under appropriate experimental conditions, despite the fact that quantitative intensity values are acknowledged to be poor. For maximum entropy methods correct phase predictions are possible for reasons described in our previous papers.[6,7,11] In the case of the simulation method, model structures can be predicted because there are so many restrictions on (a) possible molecular conformations due to restrictions in bond lengths, torsion angles, and symmetry and (b) possible crystallographic packing due to restrictions in van der Waals distances, densities and crystal symmetry.

To obtain a negative packing energy the number of possible conformations is strongly restricted. The procedure has been previously described in detail.[6–12]

2.3 High resolution imaging

High resolution images were obtained with a Philips 420 electron microscope. The samples are relatively beam sensitive so that imaging is best achieved by first adjusting the phase contrast function for transfer of the required spatial frequencies on an adjacent area of the sample as described.[6–11] Although lattice planes cannot be directly viewed on the monitor, a fast Fourier transform of the image enables a quick decision to be made regarding the suitability of the area in question for imaging and whether the correct transfer function has been chosen or not. Speed and low dose facilities are essential to prevent degradation of the sample in the electron beam.

Table 1 Experimental details of X-ray scattering for modification **B** of compound **8**

Chemical Formula	$C_{32}H_{24}$
Formula Weight	229.79
Crystal System	Trigonal
Space Group	$R\bar{3}$
Absorption Coefficient	0.53 mm^{-1}
Final R indices [$I > 2\sigma(I)$]	$R1 = 0.052$, $wR2 = 0.124$
R indices (all data)	$R1 = 0.089$, $wR2 = 0.140$
Unit Cell Dimensions	$a = 28.1031(12)$ Å
	$b = 28.1031(12)$ Å
	$c = 7.1509(4)$ Å
Cell Volume	4891.0(4) $Å^3$
Temperature of Data Collection	298(2) K
Z	9
Measured/Independent Reflections [R (int)]	2783/2234 [R (int) = 0.0431]

2.4 Generation of a molecular model

Ab initio Hartree–Fock calculations at the 3-21G level were performed.[14] The TURBOMOLE *ab initio* program package[15] was used. The geometry of an isolated molecule **8** was completely optimized and then used to build up different dimers of **8** in which only intermolecular geometrical parameters were optimized.

2.5 Simulation of electron diffraction patterns

To proceed with the simulations, the crystal unit cell and space group are required. This information is obtained from the electron diffraction data combined with X-ray powder results. Generally several space groups can be postulated on the basis of the observed extinctions. The number can normally be reduced if the symmetry requirements of the molecule and the unit cell are considered. For simulation of the diffraction pattern, the TURBOMOLE calculated molecule is placed into the unit cell with the required symmetry using CERIUS. Initial qualitative agreement and a good value of the density can generally be achieved within reasonable time. Further refinement is required to produce a negative packing energy while retaining the correct symmetry. In general an adjustment of intramolecular rotations and intermolecular distances is necessary.

2.6 X-Ray structural analysis

For X-ray analysis relatively large single crystals are required and these could not be obtained by the procedure described for electron diffraction. Instead, compound **8** was dissolved in toluene as before but was crystallized for one month at 30 °C. The modification obtained by this procedure is called **B**; later on it turned out that a third modification **C** could be obtained by a very rapid crystallization. The experimental details of the structural analysis of the crystals **B** are summarized in Table 1; for the tiny crystals of **C** only the cell parameters could be determined (Table 2).‡ The automatic solution of the crystal structure was performed by the application of the program SIR 92[16] and the refinement by the program SHELXL 97.[17]

‡ CCDC reference number 188/172. See http://www.rsc.org/suppdata/p2/1999/1881 for crystallographic files in .cif format.

Table 2 Cell parameters obtained from electron diffraction patterns (modification **A**) and from X-ray measurements (modifications **B** and **C**) of compound **8**

Modification	*a*/Å	*b*/Å	*c*/Å	*α*/°	*β*/°	*γ*/°
A	12.11	17.04	5.19	90	91.2	90
B	18.1031	28.1031	7.1509	90	90	120
C	11.902	5.300	17.312	90	100.1	90

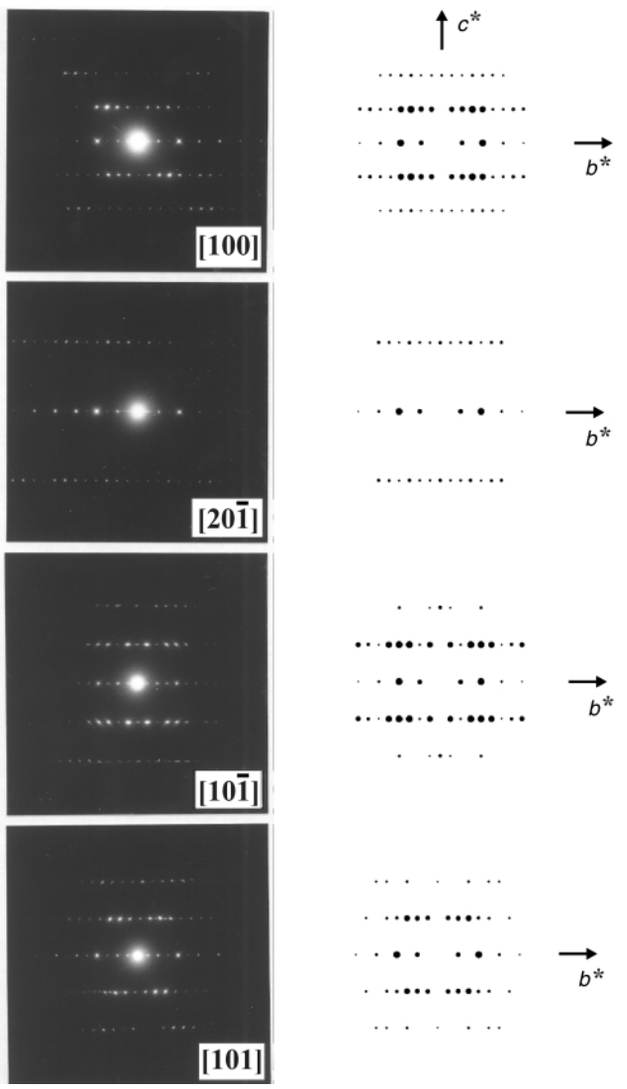

Fig. 1 Experimental electron diffraction patterns (LHS) and corresponding simulated electron diffraction patterns.

3. Results and discussion

3.1 Electron diffraction

The very small single crystals (modification **A**) were used for electron diffraction studies. The crystal was tilted about a prominent axis which was later identified as *b**. It is clear from the cell parameters found (see Table 2) that the crystals are monoclinic, and that there must be 2 molecules per unit cell to obtain a reasonable density. From the observed extinctions in the experimental diffraction patterns (Fig. 1) a $P2_1/c$ space group is likely. This implies that the two molecules should occupy special positions with the molecular inversion center coinciding with that of the crystal. The appearance of weak forbidden reflections along the *b**-axis is due to dynamical scattering. Similarly, very weak secondary scattering can be observed along the *c**-axis. Such reflections are easily recognized in organic materials and have been discussed in detail previously.[6–12]

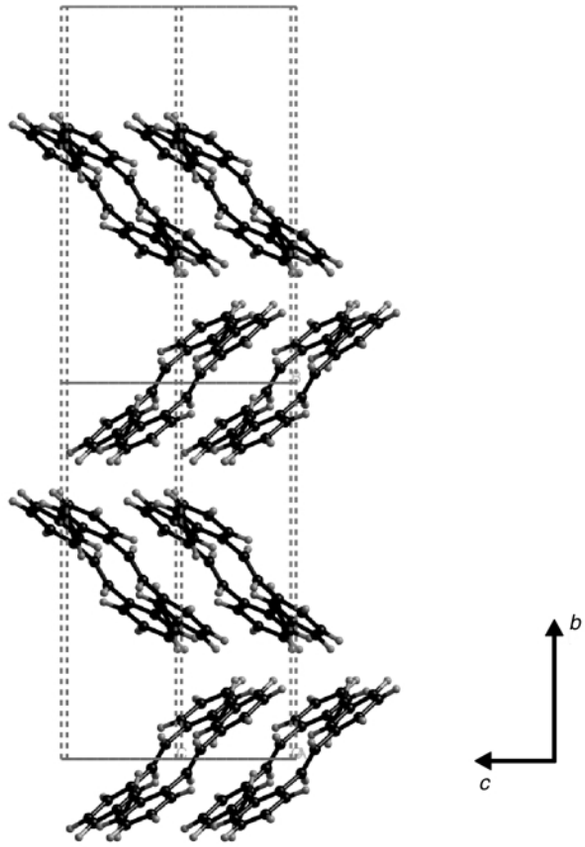

Fig. 2 Model structure used to simulate electron diffraction patterns.

Successive zones were found to be [100], [20$\bar{1}$], [10$\bar{1}$], [101]. The angles between [100] and the successive zones are +12°, +23° and −24°.

3.2 Simulation of electron diffraction patterns

Simulation of the electron diffraction patterns requires the experimental determination of the unit cell and space group. The molecule with the quantum mechanically calculated geometry is placed in the unit cell using the molecular modeling program CERIUS in such a way that the symmetry requirements based on the observed extinctions in the electron diffraction experiments are satisfied.

The packing energy is calculated by the relationship:

$$E = E_s + E_b + E_t + E_{vdW} + E_{coul} + E_{hb}$$

bonded non-bonded atoms

The packing energy was reduced by adjusting bond rotations. Finally a value of −33 kcal mol^{-1} per molecule was obtained.

Computer simulations of the possible molecular arrangement within the cell led to the crystal structure shown in Fig. 2. Using this structural model, the electron diffraction patterns were simulated for the zones which had been obtained experimentally. The results are shown in Fig. 1 together with the corresponding experimental diffraction patterns. The best agreement between theory and experiment was obtained when the final optimized geometry calculated by the *ab initio* methods was used.

In this $P2_1/c$ crystal structure, there are two parallel stacks of molecules. Within these stacks, the nearest neighboring molecules form a dimer with C_i symmetry, the CC double bonds of one molecule being placed above the double bond of the neighboring molecule (Fig. 3). The proximity of the double bonds is such as to be extremely favorable for crosslinking

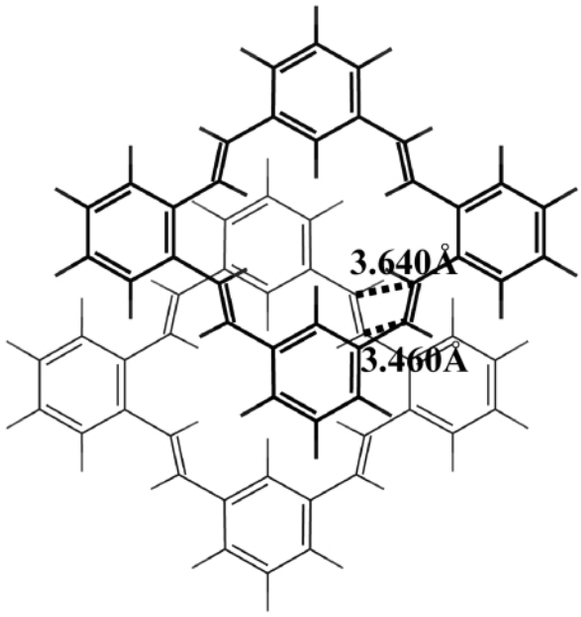

Fig. 3 Intrastack dimer with C_i symmetry used in electron diffraction simulations.

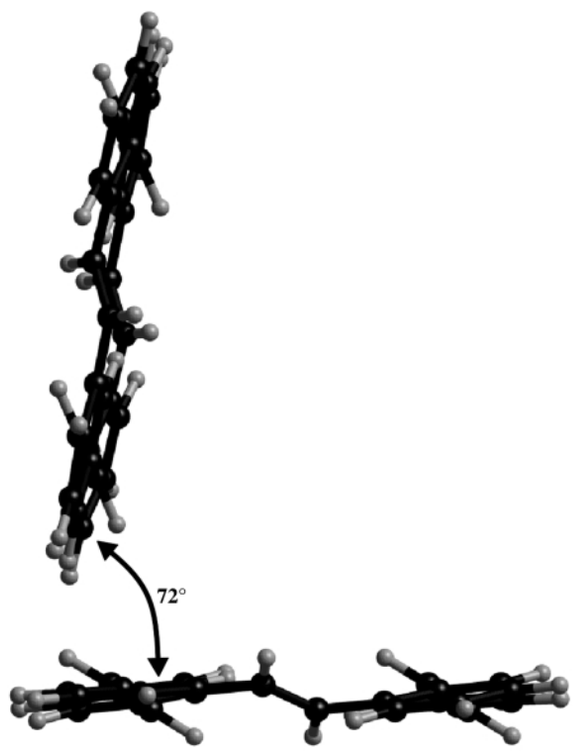

Fig. 4 Interstack dimer with C_1 symmetry obtained from electron diffraction simulations.

(*ca.* 3.5 Å), a prediction which was subsequently corroborated by the experiment. The torsion angles about the *o*-phenylene–vinylene and *m*-phenylene–vinylene bonds are 41.6° and 34.1° respectively.

Two neighboring molecules in different stacks form a molecular pair of C_1 symmetry (Fig. 4). The angle between the two molecules in these interstack pairs is 72°.

3.3 High resolution imaging

The high resolution images of the [100] projection are shown in Fig. 5b. The Figure reveals extensive areas consisting of straight lines with a separation of 17.2 Å/two lines. Inside these structures there are striations on a much smaller scale. These striations are oriented at an angle of about 42° to the lines and form an angle of about 84° to each other. The structures have a high degree of perfection.

Table 3 Results of 3-21 G *ab initio* calculations for the monomeric compound **8** and molecular pairs of **8**

Structure	Symmetry	Energy E (arbitrary units)	ΔE/kcal mol^{-1} (molecular pair formation)
Monomer	C_{2h}	−1218.894551	—
Molecular pairs	C_{2h}	−2437.791475	−4.67
	C_i	−2437.791485	−4.67
	C_2	−2437.787947	−2.46
	C_1	−2437.788246	−2.64

3.4 Simulation of image

Our model of the *bc* projection is shown in Fig. 5a. The simulated image using a slice thickness of 3.4 Å and taking account of the transfer function for a defocus value of −1000 Å and a thickness of 121.1 Å is shown in Fig. 5c. It is clear that the simulations agree well with the HRTEM image b.

3.5 X-Ray diffraction

The crystal structure determined for the large crystals **B** (Fig. 6) does not correspond to that of the small ones. These crystals belong to the $R\bar{3}$ space group (No. 148) with the cell parameters shown in Table 2. The [$\bar{5}\bar{2}2$] projection serves to demonstrate specific features which can be related to the structure determined by electron diffraction because it shows the stacking of the dimers.

The unit cell contains 9 molecules in special positions with inversion center symmetry. Thus, an individual molecule from the crystal structure is of C_i symmetry (Fig. 7a,b). The torsion angles at the *o*-phenylene–vinylene and *m*-phenylene–vinylene building blocks are 23.1° and 16.9°, respectively.

The neighboring molecules along the *c*-axis form a pair of C_i symmetry shown in Fig. 8. Within this dimer, the distance between the atoms of CC double bonds of different molecules is about 3.6 Å which also makes this crystal structure a good candidate for displaying solid-state photodimerization and photopolymerization properties (Fig. 9).

Along the *c*-axis, there are 3 parallel stacks of molecules, the neighboring molecules from different stacks forming a C_1 pair (Fig. 10). The angle between the two molecules in these pairs is 80°.

As expected, simulated electron diffraction patterns from this structure do not agree with the experimental electron diffraction patterns, confirming the result that the crystals form different polymorphs.

3.6 *Ab initio* calculations of 8

On the basis of the molecular geometry and packing determined by simulation of the electron diffraction patterns, a starting geometry for the quantum mechanical calculations was available.

The completely optimized geometry of the molecule **8** is shown in Fig. 11. It has C_{2h} symmetry and is non-planar (the total energy value is given in Table 3). The comparison of the *ab initio* optimized geometrical parameters with those found by X-ray single crystal analysis is presented in Table 4. The agreement between calculated and experimental values is very good for bond lengths and bond angles. The calculated torsion angles at the *o*-phenylene–vinylene and *m*-phenylene–vinylene building blocks are −41.6° and 35.9°, respectively. In the crystal structure determined by X-ray analysis, these angles are closer to zero (−20.9° and 11.1°, respectively). However, when the

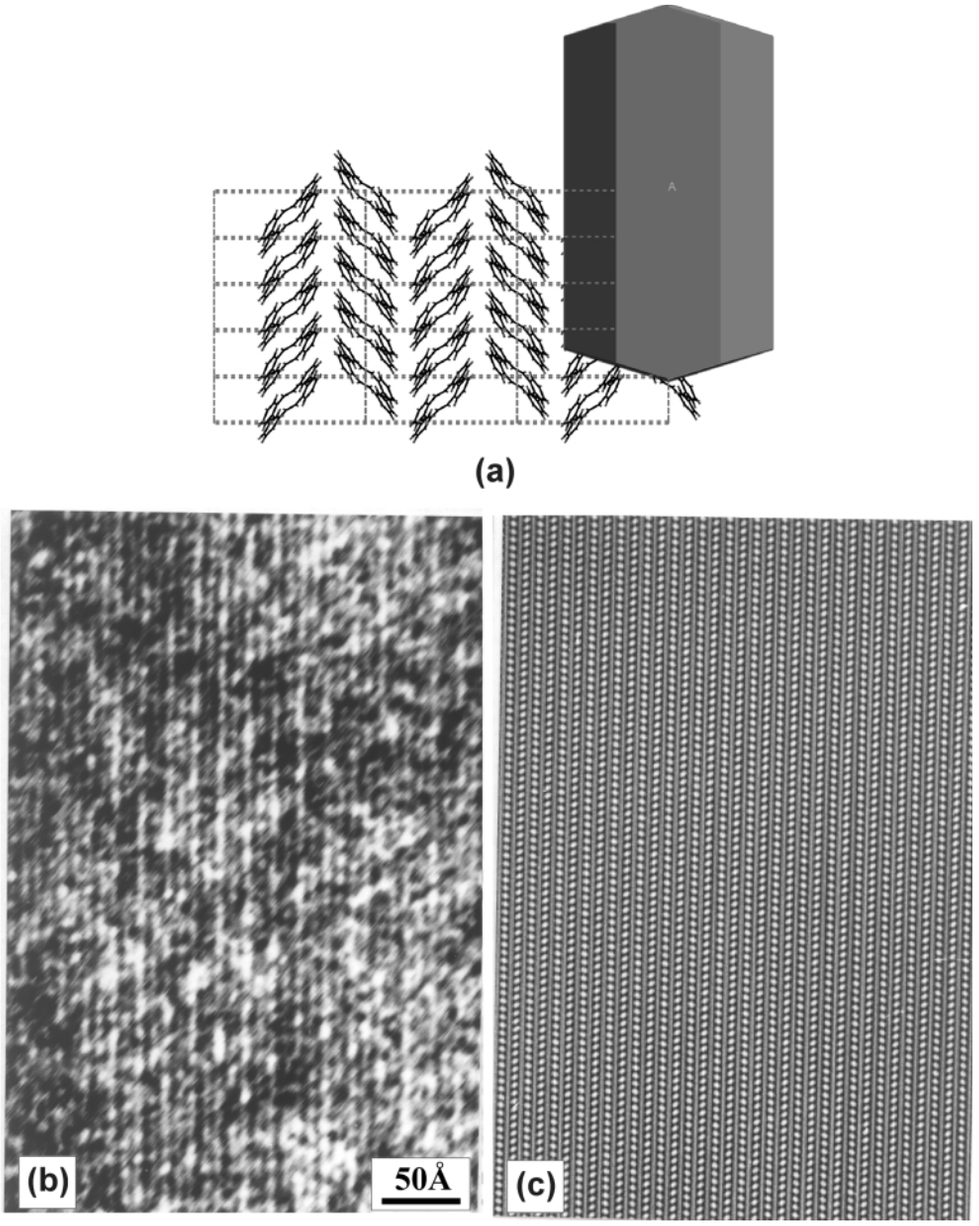

Fig. 5 Model structure (a) with high resolution image (b) and simulated image (c).

Table 4 Selected geometrical parameters of **8**

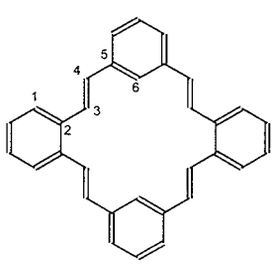

	Bond lengths/Å			Bond angles/°				Torsion angles/°	
	2-3	3-4	4-5	1-2-3	2-3-4	3-4-5	4-5-6	1-2-3-4	3-4-5-6
Ab initio calculated	1.483	1.324	1.481	120.7	124.4	124.8	121.3	−41.6	35.9
Found by X-ray analysis	1.477	1.322	1.477	120.5	126.2	125.4	121.5	−20.9	11.1

molecules in the *ab initio* optimized geometry are placed into the unit cell determined by electron diffraction, the agreement between experimental and simulated electron diffraction patterns is very good.

Dimerization was indicated by the structures determined both by electron diffraction and by X-ray diffraction. Therefore the appropriate quantum mechanical calculations were performed for molecular pairs of **8**.

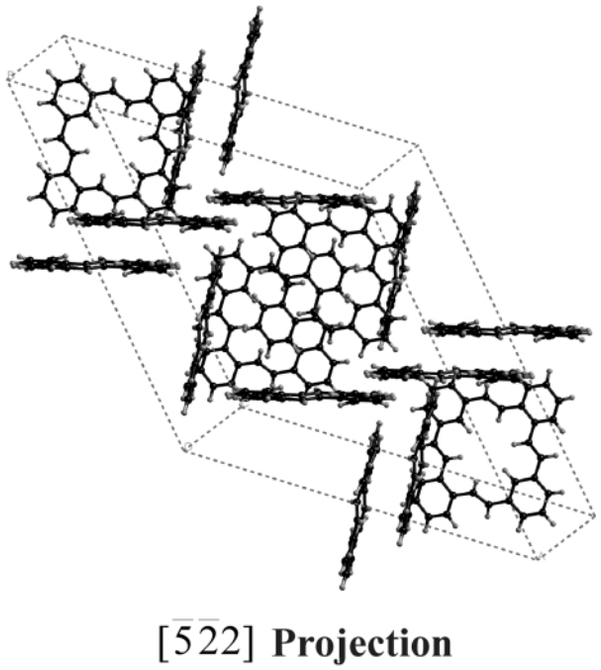

Fig. 6 Structure obtained by X-ray analysis showing [5̄2̄2] projection.

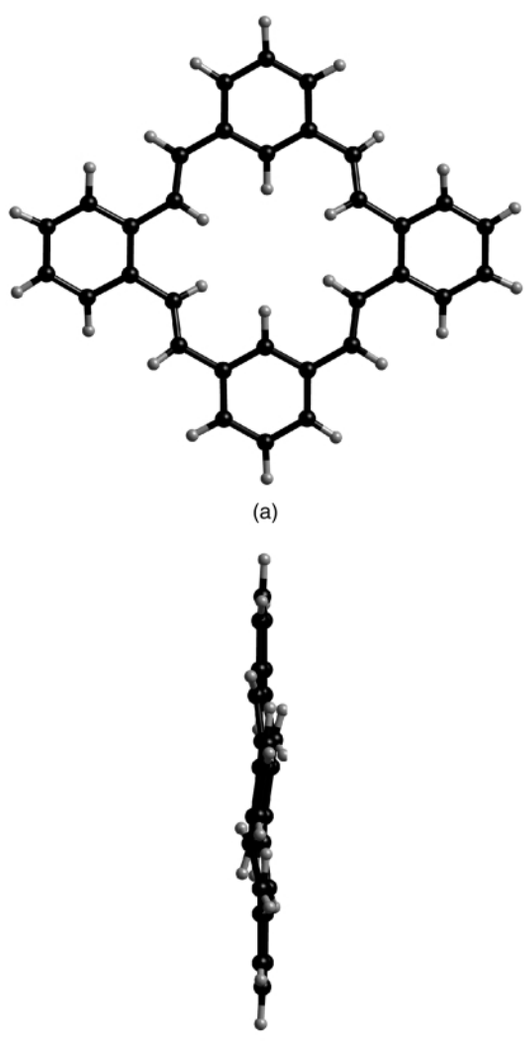

Fig. 7 Individual molecule from X-ray structure showing C_i symmetry, (a) top view; (b) side view.

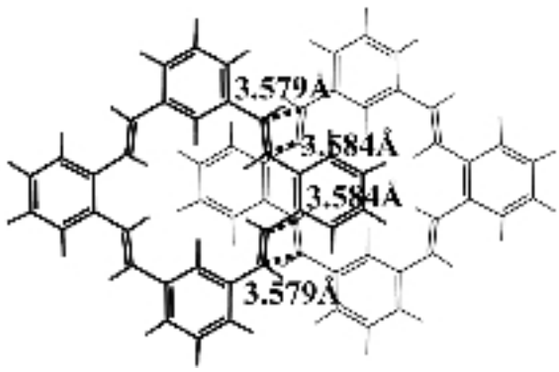

Fig. 8 Intrastack dimer with C_i symmetry from X-ray structure.

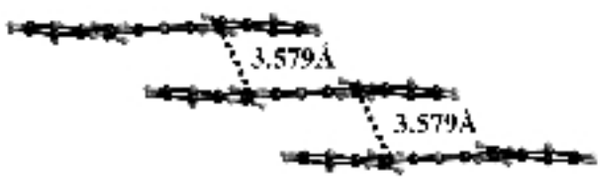

Fig. 9 Distance between molecules within stacks from X-ray structure.

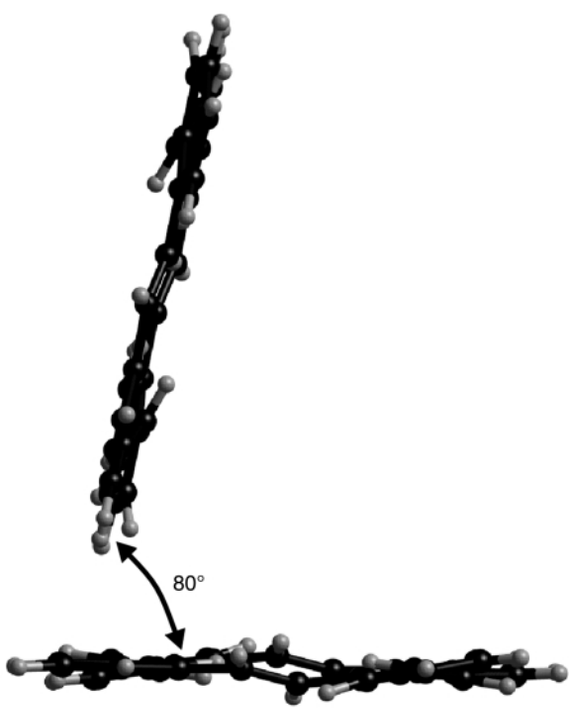

Fig. 10 Interstack dimer with C_1 symmetry from X-ray structure.

Gas-phase calculations of possible dimeric structures led to four most stable molecular pairs of C_{2h} (Fig. 12), C_i (Fig. 13), C_2 (Fig. 14) and C_1 (Fig. 15) symmetries. It can be seen from the data given in Table 3, the C_{2h} and C_i molecular pairs are of comparable stability and are more stable than the C_1 and C_2 aggregates. The energy of intermolecular attraction within the C_{2h} and C_i pairs is about 4.7 kcal mol^{-1}, which is a sufficiently high value to be able to predict definitely the stability of such dimers in solution or in the gas phase.

Within the C_{2h} molecular pair, the molecules are shifted with respect to each other so as to keep their common mirror plane (Fig. 12a). In the C_i pair, the shift is realized mainly in a direction perpendicular to that found for the C_{2h} dimer (Fig. 13a). It should be noted that in both C_{2h} and C_i aggregates, a pair of CC double bonds of one molecule is situated above the corresponding pair of the other at a distance of about 4 Å (Figs. 12b, 13b).

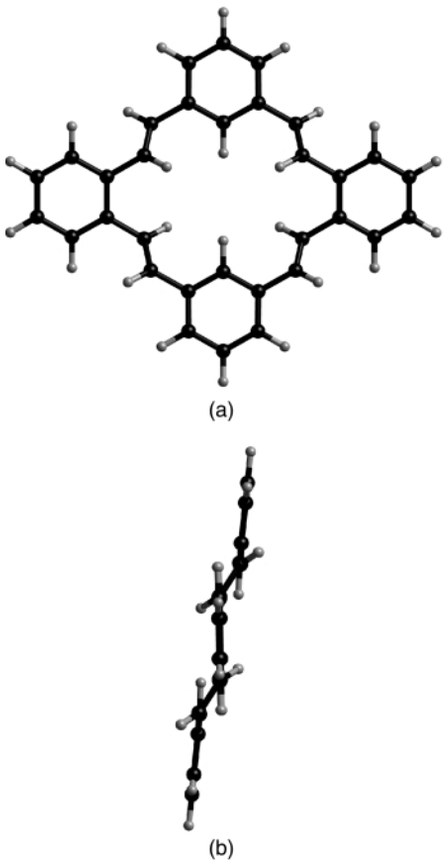

Fig. 11 Molecular conformation for C_{2h} symmetry obtained from *ab initio* calculation, (a) top view; (b) side view.

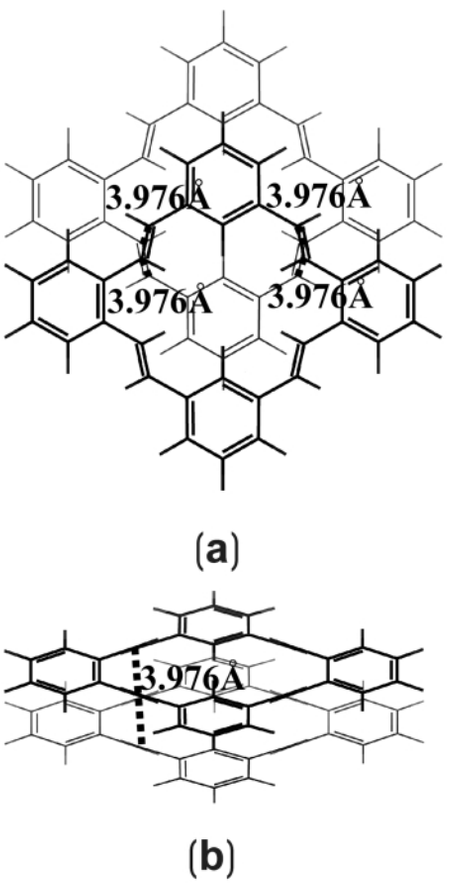

Fig. 12 Intrastack dimer in C_{2h} symmetry (*ab initio* calculations), (a) top view; (b) side view.

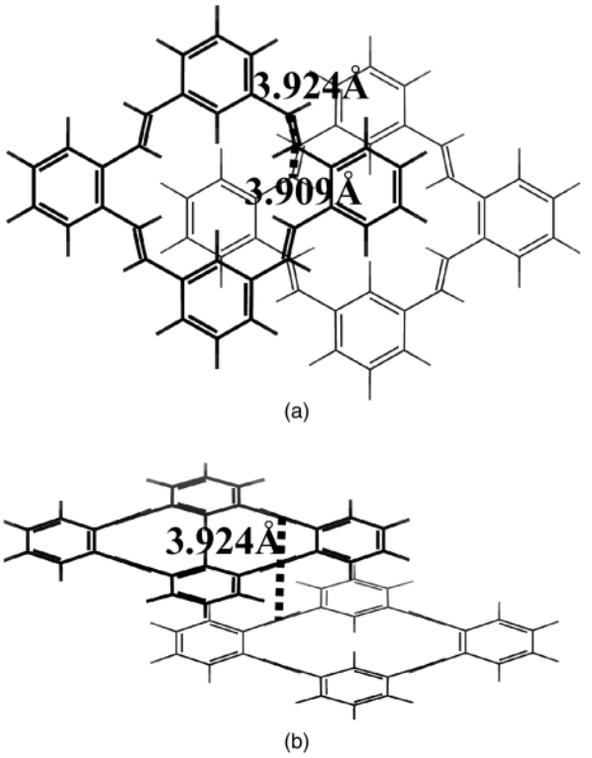

Fig. 13 Intrastack dimer in C_i symmetry (*ab initio* calculations), (a) top view; (b) side view.

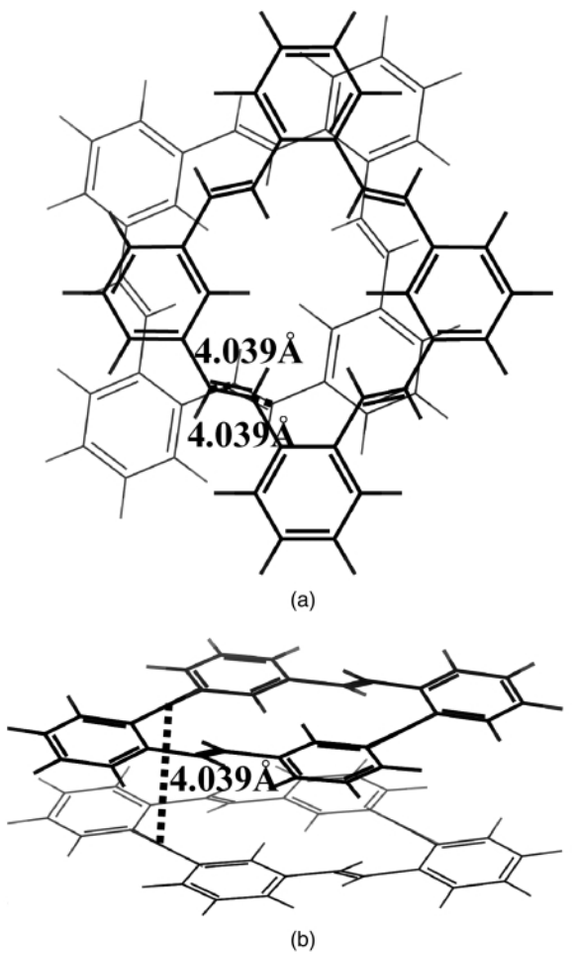

Fig. 14 Intrastack dimer in C_2 symmetry (*ab initio* calculations), (a) top view; (b) side view.

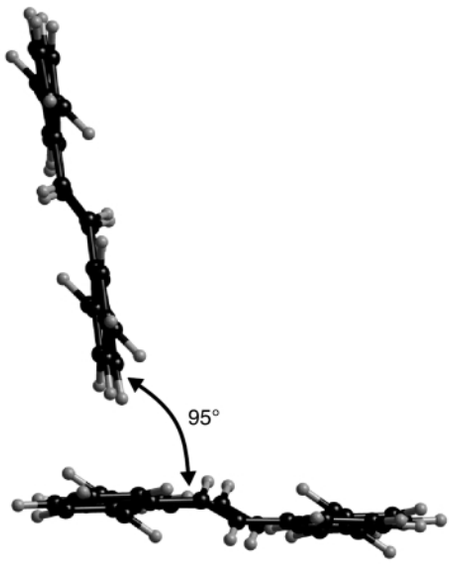

Fig. 15 Interstack dimer in C_1 symmetry (*ab initio* calculations).

Within the C_2 pair the molecules are rotated with respect to each other by about 38° (Fig. 14a). The intermolecular attraction energy is almost two times lower than in the C_{2h} and C_i pairs (Table 3). For one of the intermolecular pairs of CC double bonds the corresponding intermolecular distances between the C-atoms are also about 4 Å. However, the angle between the planes of these double bonds amounts to about 53° (Fig. 14b), making an overlap between π-orbitals less favorable.

In the C_1 molecular pair (Fig. 15), *ab initio* calculations indicate that the molecules are arranged so as to form an angle of 95° to one another.

3.7 Photochemistry

Irradiation of **8** in the polymorphous crystalline state led in a topochemical photodimerization to dimer **9** and to polymers. The short distance between the olefinic centers, *i.e.* the strong π–π-interaction enables the cycloaddition to occur (topochemical control). As soon as the first 4-membered ring is closed, the distance of the remaining double bonds is too far for further selective [2π + 2π] cycloaddition reactions. The ^{1}H NMR spectrum of **9** shows the A_2X_2 spin pattern (δ = 3.51 and 4.42) for the cyclobutane protons (C_2 symmetry) and three AB systems for the remaining olefinic protons. The coupling constants of 16 Hz prove that the original (*E*)-configurations were preserved. The unambiguous structure determination of **9** is based on the fact that only the shift of one molecule **8** with the carbon atoms C-4 and C-5 over the carbon atoms C-10 and C-11 of a second molecule **8** leads to a 4-membered ring with an A_2X_2 spin pattern. All other overlaps, like for example C-4/5 with C-22/21 of C-4/5 with C-16/15 (Scheme 1) would generate AA′XX′ spin patterns. Dimer **9** (Scheme 2) can be rationalized as the photoproduct of modification **A** and/or **C**; modification **B** as well as prolonged irradiation of all crystals led to the same result as the irradiation in solution, namely to polymerization reactions. Broad resonance signals for the methine protons in the polymer prove the CC bond formation to (different) neighboring molecules. The reaction spectra (Fig. 16) of the monochromatic irradiation in chloroform showed the almost complete disappearance of the stilbenoid ππ* band. An isosbestic point could be found at λ = 253 nm.

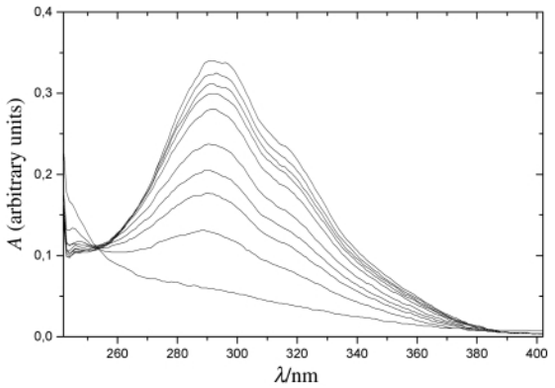

Fig. 16 Reaction spectra of the monochromatic irradiation (λ = 366 nm) of **8** in $CHCl_3$: the maximum of the absorbance *A* at 292 nm decreases almost completely within 1 h.

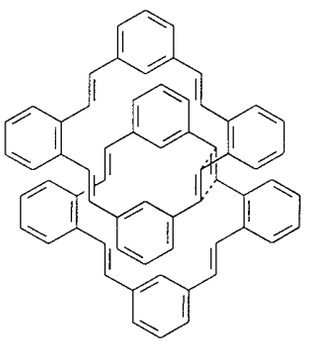

9

Scheme 2

Experimental

Synthesis and spectroscopic characterization

Melting points are uncorrected. ^{1}H and ^{13}C NMR spectra were measured in solution ($CDCl_3$ or solvent indicated) on a Bruker AM 400 spectrometer. Mass spectra were recorded in EI$^+$ made on a Finnigan MAT 95 spectrometer. The starting compound 3-bromobenzaldehyde (**3**) is commercially available.

1-Bromo-3-(dimethoxymethyl)benzene (2). Dowex 50W-X8 resin (2.0 g) was added to 3-bromobenzaldehyde (11.10 g, 60.0 mmol) in 100 cm^3 dry methanol and 50 cm^3 (459 mmol) trimethyl orthoformate. After refluxing for 2 h, the reaction mixture was cooled to ambient temperature, Na_2CO_3 (2.0 g) was added under stirring for 10 min and the volatile compounds were removed at reduced pressure. The crude product was dissolved in 100 cm^3 of hexane and filtered in order to remove the impurities. Evaporation of the hexane led to a colorless oil (12.20 g, 88%): ^{1}H NMR δ 3.30 (s, 6 H, OCH_3), 5.34 (s, 1 H, CH), 7.21 (m, 1 H, 5-H), 7.40 (m, 2 H, 4-H, 6-H), 7.60 (m, 1 H, 2-H); ^{13}C NMR δ 52.6 (OCH_3), 102.0 (CH), 122.4 (C-1), 125.3, 129.8, 129.9, 131.5 (C-2, C-4, C-5, C-6), 140.4 (C-3); MS (70 eV) *m*/*z* 232/230 (M$^+$, 7, Br pattern), 201 (98), 199 (100); $C_9H_{11}BrO_2$ (231.1) calculated C, 46.78; H, 4.80; Br, 34.58; found C, 46.69; H, 4.79; Br, 34.06%.

3-(Dimethoxymethyl)benzaldehyde (3). *n*-Butyllithium (40 cm^3 of a 1.6 M solution in *n*-hexane, 64.0 mmol) was added dropwise under argon to a solution of **2** (12.02 g, 52.0 mmol) in 200 cm^3 of dry diethyl ether which was cooled to −78 °C. The mixture was stirred for 0.5 h and then warmed to 0 °C. Dry DMF (10.0 cm^3, 130 mmol) was added, the mixture stirred for 1 h and then quenched with 50 cm^3 water. The ether layer was washed with brine, dried over $MgSO_4$, filtered and the solvent removed to yield a pale yellow oil (9.05 g, 97%): ^{1}H NMR δ 3.30 (s, 6 H, OCH_3), 5.42 (s, 1 H, CH), 7.55 (m, 1 H, 5-H), 7.68 (m, 1 H, 4-H), 7.81 (m, 1 H, 6-H), 7.94 (m, 1 H, 5-H), 9.99 (s, 1 H, CHO); ^{13}C NMR δ 52.6 (OCH_3), 102.1 (CH), 128.3, 128.9, 129.4, 132.7 (C-2, C-4, C-5, C-6), 136.1 (C-1), 139.3 (C-3), 192.1 (CHO). The crude product was directly used for the next step.

Diethyl (2-methylbenzyl)phosphonate (5). 1-Chloromethyl-2-methylbenzene (**4**) (27.04 g, 192.3 mmol) and triethyl phosphite (35.0 g, 211 mmol) were refluxed for 2 h. The excess phosphite was removed at 1 Torr (1.33×10^2 Pa) and the residue distilled between 85 and 86 °C at 0.001 Torr (1.33×10^{-1} Pa) to yield 30.0 g (64%) of a colorless oil: ^{1}H NMR δ 1.17 (t, 6 H, CH_3), 2.33 (d, ^5J (H,P) 1.6 Hz, 3 H, CH_3), 3.11 (d, ^2J (H,P) 21.9 Hz, 2 H, CH_2), 3.92 (m, 4 H, OCH_2), 7.09 (m, 3 H), 7.20 (m, 1 H) (3-H, 4-H, 5-H, 6-H); ^{13}C NMR δ 15.8 (d, ^3J (C,P) 5.9 Hz, CH_3), 19.3 (2-CH_3), 30.5 (d, ^1J (C,P) 138.2 Hz, CH_2), 61.4 (d, ^2J (C,P) 6.7 Hz, OCH_2), 125.4 (d, ^4J (C,P) 3.0 Hz, C-3), 126.4 (d, ^4J (C,P) 3.5 Hz, C-5), 129.5 (d, ^2J (C,P) 9.4 Hz, C-1), 129.8 (d, ^5J (C,P) 2.7 Hz, C-4), 130.0 (d, ^3J (C,P) 5.5 Hz, C-6), 136.3 (d, ^3J (C,P) 6.5 Hz, C-2); MS (70 eV) *m*/*z* 242 (M^+, 48), 186 (33), 105 (100); $C_{12}H_{19}O_3P$ (242.3), calculated C, 59.50; H, 7.91; found C, 59.38; H, 7.79%.

(*E*)-3-[2-(2-Methylphenyl)ethenyl]benzaldehyde (6). To a solution of **5** (9.69 g, 40.0 mmol) in 100 cm^3 1,2-dimethoxyethane (DME) NaH (3.84 g, 160.0 mmol) was added under argon. The mixture was refluxed for 20 min followed by dropwise addition of **3** (8.73 g, 48.4 mmol) dissolved in 50 cm^3 of dry DME. After further refluxing for 1 h, the reaction mixture was cooled, quenched carefully with 20 cm^3 of methanol and poured into a stirred mixture of 200 cm^3 ether and 100 cm^3 2 M HCl. After 2 h the organic layer was separated, washed with 50 cm^3 saturated $NaHCO_3$ solution, dried over $MgSO_4$ and filtered. Removal of the solvent gave an oil which was chromatographed on silica gel using dichloromethane as eluant. A pale yellow oil (4.79 g, 54%) was isolated: ^{1}H NMR δ 2.44 (s, 3 H, CH_3), 7.02, 7.43 (AB, ^3J 16.2 Hz, 2 H, olefin. H), 7.20 (m, 3 H, arom. H), 7.51 (m, 2 H, arom. H), 7.75 (m, 2 H, arom. H), 8.01 (m, 1 H, 2-H), 10.04 (s, 1 H, CHO); ^{13}C NMR δ 19.9 (CH_3), 125.4, 126.2, 127.1, 128.0, 128.2, 128.3, 128.8, 129.3, 130.4, 132.3 (arom. and olefin. CH), 135.7, 135.9, 136.7, 138.5 (arom. C_q), 192.2 (CHO); MS (70 eV): *m*/*z* 222 (M^+, 100), 193 (26), 178 (59); $C_{16}H_{14}O$ (222.3) calculated C, 86.45; H, 6.35; found C, 86.50; H, 6.43%.

(*E*,*E*)-3-[2-(2-Methylphenyl)ethenyl]-*N*-phenylbenzaldimine (7). Aniline (2.33 g, 25.0 mmol) and **6** (4.58 g, 20.6 mmol) were heated with stirring for 2 h at 60 °C. During the reaction the generated water was several times removed at 15 Torr (2.0×10^3 Pa). After the condensation had come to an end, excess aniline was evaporated at 0.01 Torr (1.33 Pa) to leave 6.13 g (100%) of a yellow viscous oil which was analytically pure. ^{1}H NMR δ 2.45 (s, 3 H, CH_3), 7.05, 7.41 (AB, ^3J 16.2 Hz, olefin. H), 7.21 (m, 6 H, arom. H), 7.41 (m, 2 H, arom. H), 7.49 (m, 1 H, arom. H), 7.62 (m, 2 H, arom. H), 7.77 (m, 1 H, arom. H), 8.07 (m, 1 H, 2-H), 8.49 (s, 1 H, CHN); ^{13}C NMR δ 19.9 (CH_3), 120.8, 125.4, 126.0, 126.2, 126.5, 127.4, 127.7, 128.1, 129.0, 129.1, 129.2, 129.3, 130.4 (arom. and olefin. H), 135.9, 136.1, 136.5, 138.2 (arom. C_q), 151.9 (C_q-N), 160.2 (CH=N); MS (70 eV) *m*/*z* 297 (M^+, 14), 110 (100), 93 (64); $C_{22}H_{19}N$ (297.4) calculated C, 88.85; H, 6.44; N, 4.71; found C, 88.71; H, 6.42; N, 4.77%.

(4*E*,10*E*,15*E*,21*E*)-Tetrabenzo[*ab*,*f*,*jk*,*o*]cyclooctadecene (tetrabenzo[*ab*,*f*,*jk*,*o*][18]annulene) (8). Dry DMF (150 cm^3) was degassed several times and heated under argon to 80–90 °C. Potassium *tert*-butoxide (9.32 g, 83.05 mmol) was slowly added with vigorous stirring followed by a dropwise addition of **7** (4.94 g, 16.61 mmol) in 200 cm^3 of dry DMF. The mixture turned violet and was stirred for 1.5 h at 90 °C. After cooling to ambient temperature, 100 cm^3 of water and 100 cm^3 of 2 M HCl were added. The formed yellowish–brown precipitate was sucked off, washed first with 200 cm^3 water, then with 50 cm^3 methanol and 20 cm^3 acetone and finally with 20 cm^3 pentane to yield 1.24 g (37%) of a beige solid which could be recrystallized from toluene, mp >300 °C: IR (KBr) $\tilde{\nu}$/cm^{-1} 3050, 1590, 1485, 1315, 960, 780, 755, 690; ^{1}H NMR ($C_2D_2Cl_4$, 400 MHz) δ 7.08 (d, ^3J 16.1 Hz, 4 H, 4-H), 7.20 (m, 4 H, 1-H), 7.27 (m, 4 H, 7-H), 7.32 (t, 2 H, 2-H), 7.70 (m, 4 H, 6-H), 7.83 (d, ^3J 16.1 Hz, 4 H, 5-H), 8.29 (d, 2 H, 23-H); the correlation of the signals was achieved by NOE measurements. The low solubility of **8** in usual NMR solvents did not permit the measurement of a ^{13}C NMR spectrum. MS (70 eV) *m*/*z* 408 (M^+, 100), 204 (M^{2+}, 14); $C_{32}H_{24}$ (408.5) calculated C, 94.08; H, 5.92; found C, 93.80; H, 6.04%.

Photodimerization of 8

A suspension of 16.0 mg (0.04 mmol) **8** in 500 ml water was circulated through a photoreactor equipped with a 150 W mercury lamp (Hanau TQ 150 Z 3) with a main emission between 300 and 400 nm. After 1 h the irradiation was stopped and the suspension filtered. The dry residue was dissolved in $CDCl_2$–$CDCl_2$. The ^{1}H NMR spectrum at 323 K shows the signals of **8** and its dimer **9** in a ratio of 30 : 70 and a small amount of oligomers. Prolonged irradiation yielded higher amounts of oligomeric material. **9**: ^{1}H NMR ($C_2C_2Cl_4$): δ = 3.51, 4.42 (A_2X_2, 4 H, cyclobutane ring); 6.10, 6.42, 6.46 (3 d, ^3J = 16 Hz, 6 H, A parts of three olefin. AB systems), 6.70–7.80 (m, 34 H, arom. H and B parts of AB systems), 7.89 ("s", 2 H, arom. H), 8.22 ("s", 2 H, arom. H). MS (FD): *m*/*z* (%) = 816 (31) [$M^{+\bullet}$], 652 (85), 408 (100).

Conclusions and outlook

Disc-like areno-condensed annulenes exhibit a high aggregation tendency in solution, in mesophases and in the solid state.[2] We studied this phenomenon in the solid state for the model compound **8** which crystallizes in three different modifications. The results discussed above show that gas phase *ab initio* calculations predict reasonable dimeric structures of **8** which agree, in most of the essential features, with those found in crystals. However, some important intermolecular parameters, such as the precise shift of molecules in specific directions, are influenced by the crystal field. Therefore a combination of both methods is essential in order to understand solid state properties. Subsequent gas-phase *ab initio* quantum-chemical calculations of the intermolecular interaction within different molecular pairs are important in order to obtain information about possible physical effects such as arrangement and order in liquid crystalline (LC) phases, photoconductivity or photopolymerization and photocrosslinking. Irrespective of a topochemical photodimerization **8**→**9**, all crystal modifications of **8** enter a polymerization on irradiation. The arrangement of neighboring molecules in the crystal structures found is, in principle, suitable for photoconductivity as well as for photocrosslinking properties. However, photocrosslinking in the crystal state is rather probable due to the very close distance (*ca.* 3.5 Å) of double bonds of neighboring molecules. This photocrosslinking would destroy the π-conjugation in a part of the molecule and can, thus, prevent or reduce the photoconductivity. However, in the liquid crystalline state, photocrosslinking is much less probable during the singlet excited state lifetime. The fluorescence lifetimes of similar [18]annulenes condensed with aromatic ring systems were measured to be less than 10 ns.[2] In that case, photoconductivity may become a dominating physical property if a stacking (columnar) arrangement of molecules survives.

The crystal structures found by electron diffraction and X-ray analysis are different polymorphs with strongly favorable negative crystal packing energies. The total packing energies of the small crystals whose structure was determined by electron diffraction are −33 and −38 kcal mol^{-1} per molecule for the structures simulated with the *ab initio* gas-phase conformation and conformation taken out from the X-ray structure. The van der Waals energy of the large crystals is −47 kcal mol^{-1} per molecule. These values are sufficiently close to one another to explain the polymorphism.

Acknowledgements

The authors gratefully acknowledge financial support by the Deutsche Forschungsgemeinschaft and by the Fonds der Chemischen Industrie.

References

1 H. Meier and K. Müller, *Angew. Chem.*, 1995, **107**, 1598; *Angew. Chem., Int. Ed. Engl.*, 1995, **34**, 1003.
2 K. Müller, H. Meier, H. Bouas-Laurent and J. P. Desvergne, *J. Org. Chem.*, 1996, **61**, 5474.
3 H. Kretzschmann, K. Müller, H. Kolshorn, D. Schollmeyer and H. Meier, *Chem. Ber.*, 1994, **127**, 1735.
4 H. Meier, K. Müller and M. Fetten, *J. Inf. Rec.*, 1996, **22**, 421.
5 H. Meier, Th. Lifka and K. Müller, *J. Inf. Rec. Mater.*, 1994, **21**, 457.
6 I. G. Voigt-Martin, D. H. Yan, C. Gilmore, K. Shankland and G. Bricogne, *Ultramicroscopy*, 1994, **56**, 271.
7 I. G. Voigt-Martin, D. H. Yan, A. Yakimansky, D. Schollmeyer, C. J. Gilmore and G. Bricogne, *Acta Crystallogr., Sect. A*, 1995, **51**, 849.
8 I. G. Voigt-Martin, Li Gao, A. Yakimanski, G. Schulz and J. J. Wolff, *J. Am. Chem. Soc.*, 1996, **118**, 12830.
9 I. G. Voigt-Martin, Z. X. Zhang, D. H. Yan, A. Yakimanski, R. Wortmann, R. Matschiner, P. Krämer, C. Glania and N. Detzer, *Colloid Polym. Sci.*, 1997, **275**, 18.
10 A. V. Yakimanski, I. G. Voigt-Martin, U. Kolb, G. N. Matveeva and Z. X. Zhang, *Acta Crystallogr., Sect. A*, 1997, **53**, 603.
11 I. G. Voigt-Martin, Z. X. Zhang, U. Kolb and C. Gilmore, *Ultramicroscopy*, 1997, **68**, 43.
12 I. G. Voigt-Martin, Gao Li, A. Yakimanski, J. J. Wolff and H. Gross, *J. Phys. Chem.*, 1997, **A 101**, 7265.
13 D. Dorset, *Structural Electron Microscopy*, Plenum Press, New York and London, 1995.
14 J. S. Binkley, J. A. Pople and W. J. Hehre, *J. Am. Chem. Soc.*, 1980, **102**, 939.
15 R. Ahlrichs, M. Bär, M. Häser, H. Horn and C. Kölmel, *Chem. Phys. Lett.*, 1989, **162**, 165.
16 A. Altomare, G. Cascarano, C. Giacovazzo, A. Guagliardi, M. C. Burla, G. Polidori and M. Camalli, *J. Appl. Crystallogr.*, 1994, **27**, 435.
17 G. M. Sheldrick, SHELXL 97, *Program for crystal structure refinement 1997*, University of Göttingen, Germany.

Paper 9/03451J